A Versatile 3R Pseudo-Rigid-Body Model for Initially Curved and Straight Compliant Beams of Uniform Cross Section

Venkatasubramanian Kalpathy Venkiteswaran
Department of Biomechanical Engineering,
University of Twente,
Drienerlolaan 5,
Enschede 7522 NB, The Netherlands
e-mail: v.kalpathyvenkiteswaran@utwente.nl

Hai-Jun Su
Department of Mechanical and
Aerospace Engineering,
The Ohio State University,
Columbus, OH 43210
e-mail: su.298@osu.edu

Rigid-body discretization of continuum elements was developed as a method for simplifying the kinematics of otherwise complex systems. Recent work on pseudo-rigid-body (PRB) models for compliant mechanisms has opened up the possibility of using similar concepts for synthesis and design, while incorporating various types of flexible elements within the same framework. In this paper, an idea for combining initially curved and straight beams within planar compliant mechanisms is developed to create a set of equations that can be used to analyze various designs and topologies. A PRB model with three revolute joints is derived to approximate the behavior of initially curved compliant beams, while treating straight beams as a special case (zero curvature). The optimized model parameter values are tabled for a range of arc angles. The general kinematic and static equations for a single-loop mechanism are shown, with an example to illustrate accuracy for shape and displacement . Finally, this framework is used for the design of a compliant constant force mechanism to illustrate its application, and comparisons with finite element analysis (FEA) are provided for validation. [DOI: 10.1115/1.4040628]

1 Introduction

The functionality and performance of compliant mechanisms are deeply intertwined with the relationship between the loads acting on them and the deformation of their parts [1,2]. When the deformation under study is limited to instantaneous or small values, the analysis can often be performed using matrix algebra and screw theory [3–7]. However, when large deformation analysis is necessary, the methods used include beam theory [8,9], finite element analysis (FEA) [10,11], and pseudo-rigid-body (PRB) models [12,13].

Pseudo-rigid-body models are numerical approximations of compliant members that can be used for large deformation analysis. The kinematics are defined using rigid-body transformations, with spring elements to mimic the elastic properties of the material. There has been significant work in this area over the past two decades, although much of it was focused on individual applications rather than toward a generic approach. PRB models have been derived for various types of compliant elements, such as fixed-guided beams [14,15], curved segments [16,17], cross-strip pivots [18], and straight beams under bending [19,20]. Recent work also focused on PRB models for soft joints with extension effects [21,22].

The main motivation behind this work is to demonstrate the use of PRB models for general design of compliant mechanisms, using different types of flexure elements. This is possible because the numerical values in PRB models can represent different deformation characteristics. However, in order to achieve this, it is necessary to create a framework for deriving and solving statics and kinematics equations, which can preferably be automated for use with computers. Additionally, PRB models have been demonstrated to have fast analysis times [23], which will help with iterative evaluations during synthesis, or even real-time control.

The use of curved beams in compliant mechanism design is rather limited, even though they do offer certain advantages [24–26]. Apart from a different geometrical shape, they can also offer a degree-of-freedom (and a corresponding stiffness) between their two end points, whereas straight beams tend to act more like constraints. This idea is illustrated in Fig. 1, and may be utilized to good effect in design. Therefore, combining the speed and versatility of PRB models with the usage of curved and straight beams can be advantageous for the design of compliant mechanisms. Other researchers have worked on PRB models for curved beams previously, although these were aimed at specific loading cases. Pinned–pinned circular beams were analyzed by Edwards et al., but that cannot include moment loads [16]. Wang et al. used a single-DOF model for approximating pivot-type motions of semi-circular segments [27]. Kuber worked on models specific to individual loading conditions [28]. The model derived here will be suitable for general loads, for initially curved beams of a large range of arc angles, although it is limited to slender beams of uniform cross section for planar applications. Other salient contributions of this paper are the representation of curved and straight beams within a single model and a framework for synthesis that utilizes its potential to achieve realistic designs.

In Sec. 2, the derivation of the PRB model for curved and straight beams will be explained. The various PRB parameters will be defined and the results shown for beams of arc angles from 0 deg (straight beam) to 270 deg. Following that, the equations for analyzing a single-loop fully compliant mechanism will be detailed in Sec. 3, along with the solution process and accuracy validation. In Sec. 4, the theoretical design of a compliant constant-force mechanism will be explained, to illustrate the use of the equations and the PRB models. Section 5 will then discuss some of the advantages and drawbacks of this method.

2 The Versatile 3R Pseudo-Rigid-Body Model

In this section, a PRB model will be derived, which can be used to represent both initially curved and straight beams. The model is capable of analyzing beam-like elements with a uniform cross section and a high length-to-width ratio. The model incorporates forces and moments acting at the tips, which will be necessary for use within a mechanism where beams are rigidly connected to one

Contributed by the Mechanisms and Robotics Committee of ASME for publication in the Journal of Mechanical Design. Manuscript received February 8, 2018; final manuscript received June 9, 2018; published online July 9, 2018. Assoc. Editor: Dar-Zen Chen.

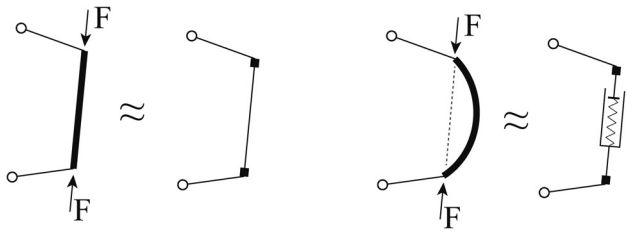

Fig. 1 A straight beam can act as a line constraint between two points (assuming no buckling), whereas a curved beam has behavior similar to a stiff prismatic joint

another. For simplicity, it is assumed that the beams undergo only lateral bending under the action of the loads, and therefore, the Euler–Bernoulli beam equations are used to calculate their deflections. The PRB model is then defined to mimic the deflection obtained from the beam theory approach by optimizing the values of its parameters. The objective is to minimize the error between the model and the results from beam theory [29].

2.1 Beam Equations. An initially curved cantilever beam subject to tip loads F (at an angle Φ) and moment M is shown in Fig. 2. The beam has a cross section with second moment of area, I and is made of a material with elastic modulus E. The constant initial radius of curvature is R, and the angle subtended by it is ψ. The length of the beam $L = \psi R$. If s is the coordinate along the arc length and $\theta(s)$ is the slope, the differential equations and boundary conditions that define the behavior of the beam under the action of the loads are

$$\theta''(s) = \alpha \sin(\theta - \Phi) \quad s \in [0, L] \tag{1}$$

$$\theta(0) = 0 \quad \theta'(L) = \beta + \kappa \tag{2}$$

where

$$\alpha = \frac{FL^2}{EI} \quad \beta = \frac{ML}{EI} \quad \kappa = \frac{1}{R} = \frac{\psi}{L}$$

It is worth noting that a straight beam is just a special case of this, where the initial curvature, κ, is zero. Thus, the deflection of both straight and curved beams can be calculated using these equations.

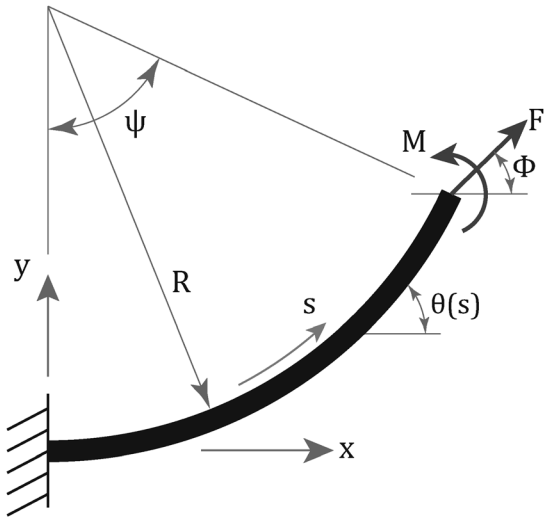

Fig. 2 Initially curved beam subject to tip loads

2.2 Definition of the Pseudo-Rigid-Body Model. The PRB models used here consist of four rigid segments with three revolute joints. A schematic of the model is shown in Fig. 3. The model is chosen to have three joints to match the three independent degrees-of-freedom for planar motion, which results in a square Jacobian in the mapping from the joint space to the actuation space (described later). The three degrees-of-freedom in the model allow for estimation of the beam deflection with high accuracy, as demonstrated in previous work on straight beams [23].

The model is defined to be symmetric about the central joint such that the lengths and stiffness on either side of it are the same. The symmetry allows the beams to have their fixed or free ends on either side without loss of accuracy (which is not the case for other asymmetric models in literature). This has two advantages: (1) it allows the usage of the models for graph-based analysis of compliant mechanisms [23], and (2) it decreases the number of PRB parameters to be determined, which reduces the computation. Each revolute joint has a stiffness $K_{\theta i}$, and each segment has a length $\gamma_i L$. Each rigid segment is at an angle ζ_i from the previous segment in the undeflected position, and this angle is zero for straight beams. An additional rule enforced here is that the revolute joints must be on the circular arc in the undeformed configuration, which is key for compatibility between straight and curved beams.

If the beam at the fixed end is tangential to the X axis, the tip coordinates of the model under deformation are given by

$$X_{\text{tip}} = L \sum_{j=1}^{4} \cos\left[\sum_{i=1}^{j}(\zeta_i + \theta_i)\right]\gamma_j \tag{3}$$

$$Y_{\text{tip}} = L \sum_{j=1}^{4} \sin\left[\sum_{i=1}^{j}(\zeta_i + \theta_i)\right]\gamma_j \tag{4}$$

$$\theta_{\text{tip}} = \psi + \theta_2 + \theta_3 + \theta_4 \tag{5}$$

where θ_i is the rotation of the ith segment, with $\theta_1 = 0$ always (for a beam with a cantilever support). From geometry, a mathematical relationship can be calculated between γ_i and ζ_i as given below:

$$\gamma_1 = -\frac{2}{\psi}\frac{\sin(\psi/4)\sin(\psi/4 - \zeta_1 - \zeta_2)}{\sin\zeta_2} \tag{6}$$

$$\gamma_2 = \frac{2}{\psi}\frac{\sin(\psi/4)\sin(\psi/4 - \zeta_1)}{\sin\zeta_2} \tag{7}$$

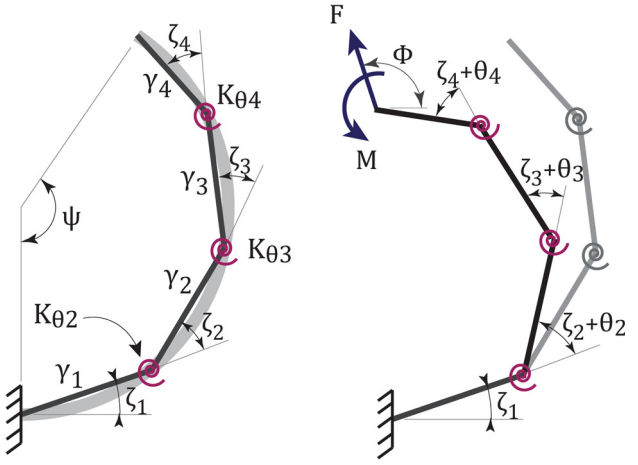

Fig. 3 Symmetric 3R PRB model for initially curved beams before and after deformation

Due to the symmetry in the definition of the PRB model, a few other expressions can be derived

$$\gamma_4 = \gamma_1 \quad \gamma_3 = \gamma_2 \quad \zeta_4 = \zeta_2 = \frac{\psi}{4}$$

Since all joints are on the beam in the undeflected position, a few more relations can be added

$$\gamma_1 = \frac{2}{\psi} \quad \gamma_2 = \frac{2}{\psi}\sin\left(\frac{\psi}{4} - \zeta_1\right) \quad \zeta_3 = \frac{\psi}{2} - 2\zeta_1$$

The spring stiffness values are also symmetric: $K_{\theta 2} = K_{\theta 4}$.

The statics of the PRB model under the action of tip loads is defined by Craig [30]

$$\boldsymbol{\tau} = \mathbf{J}^{\mathrm{T}}\mathbf{W} \tag{8}$$

where τ represents the internal moments at the joints given by

$$\boldsymbol{\tau} = \begin{Bmatrix} K_{\theta 2}\theta_2 \\ K_{\theta 3}\theta_3 \\ K_{\theta 4}\theta_4 \end{Bmatrix}$$

and W represents the components of the external loads given by

$$\mathbf{W} = \begin{Bmatrix} |F|\cos\Phi \\ |F|\sin\Phi \\ M \end{Bmatrix}$$

The matrix J is the Jacobian of the mapping from the configuration of the PRB model (defined by the set of joint angles, $(\theta_i : i \in \{2,3,4\})$ to the tip coordinates defined in Eqs. (3)–(5)

$$\mathbf{J} = \begin{bmatrix} \frac{\partial X_{\mathrm{tip}}}{\partial \theta_2} & \frac{\partial X_{\mathrm{tip}}}{\partial \theta_3} & \frac{\partial X_{\mathrm{tip}}}{\partial \theta_4} \\ \frac{\partial Y_{\mathrm{tip}}}{\partial \theta_2} & \frac{\partial Y_{\mathrm{tip}}}{\partial \theta_3} & \frac{\partial Y_{\mathrm{tip}}}{\partial \theta_4} \\ \frac{\partial \theta_{\mathrm{tip}}}{\partial \theta_2} & \frac{\partial \theta_{\mathrm{tip}}}{\partial \theta_3} & \frac{\partial \theta_{\mathrm{tip}}}{\partial \theta_4} \end{bmatrix}$$

The deformation of the PRB model under the action of tip loads is determined by solving Eq. (8) to obtain θ_2, θ_3, and θ_4.

2.3 Calculation of Pseudo-Rigid-Body Parameters. Using the above equations, a numerical optimization procedure is employed to calculate the optimal values of the PRB parameters over a large range of loading cases. The idea is to minimize the average error in the estimation of the tip deflection using the PRB model compared to the beam equations [29].

The joint stiffness values are defined as

$$K_{\theta i} = k_{\theta i}\frac{EI}{L} \quad i = 2,3,4$$

and $k_{\theta i}$ are used as the PRB parameters. The model has three independent PRB parameters, namely $k_{\theta 2}, k_{\theta 3}$, and ζ_1. All other geometrical parameters can be derived from ζ_1 using the expressions described in Sec. 2.2, while $k_{\theta 4} = k_{\theta 2}$. The use of the dimensionless parameters $k_{\theta i}$ and γ_i allows scaling of the model to be used with other materials and geometries.

In the work presented here, only beams with arc angles up to 270 deg or $3\pi/2$ rad are studied. This is because incorporating beams beyond this limit would be difficult and perhaps impractical from the point of view of design. The PRB parameters were optimized over the range of loads

$$\alpha \in [-1.5, 1.5] \quad \beta \in [-0.75, 0.75] \quad \Phi \in \left[-\frac{\pi}{2}, \frac{\pi}{2}\right]$$

and the results are presented in Table 1. The results are also presented in graphical form in Fig. 4. The load values were chosen to generate results that reflect large deformations of the beams (greater than 90 deg) for different loading conditions. The PRB model estimates the tip deflection with an average error of less than 0.6% (compared to the values from beam theory) for the entire range of beam arc angles.

Note that the value of γ_1 was obtained using Eq. (6), but is tabulated for easier visualization of the PRB model. The optimal values of the parameters were fit to a polynomial curve of the form $C_0 + C_1\psi + C_2\psi^2 + C_3\psi^3 + C_4\psi^4$. This provides a direct mapping from the arc angle, allowing easy use during the design process. The values of the coefficients are given in Table 2.

Table 1 Optimal values of PRB parameters compared to beam equations for circular beams with angle of curvature between 0 deg and 270 deg. The PRB parameters were optimized over the range of loads $\alpha \in [-1.5, 1.5]$, $\beta \in [-0.75, 0.75]$ and $\Phi \in [(-\pi/2), (\pi/2)]$.

ψ (deg)	ζ_1	γ_1	$k_{\theta 2} = k_{\theta 4}$	$k_{\theta 3}$
0	0	0.1337	3.1567	2.7389
15	0.0174	0.1329	3.1735	2.7132
30	0.0339	0.1294	3.2388	2.621
45	0.0502	0.1277	3.2722	2.5769
60	0.0666	0.1271	3.2944	2.5491
75	0.0824	0.1257	3.326	2.5117
90	0.0979	0.1244	3.3519	2.483
105	0.1126	0.1226	3.3872	2.4456
120	0.1292	0.123	3.3894	2.4432
135	0.1456	0.1231	3.3966	2.4352
150	0.1625	0.1235	3.3955	2.4349
165	0.1812	0.1251	3.3768	2.4528
180	0.2008	0.1269	3.3546	2.4764
195	0.2217	0.1292	3.3235	2.5106
210	0.243	0.1313	3.2944	2.5439
225	0.2641	0.1329	3.2727	2.5706
240	0.2859	0.1346	3.2517	2.5973
255	0.3085	0.1364	3.2314	2.6233
270	0.3342	0.1392	3.2011	2.6629

3 Equations for a Compliant Mechanism

With the PRB models as defined in Sec. 2, it is now possible to set up the framework for the derivation of kinematic loop equations, and also the equations defining the static equilibrium of a compliant mechanism. In order to automate the process, it is necessary to create a few naming conventions, which are described as follows.

Consider a single-loop compliant mechanism with a few straight and curved compliant beams as shown in Fig. 5. The figure also shows the pth beam from an arbitrary starting point within the loop, between the points P and Q (bottom). As a convention, the loop is analyzed in the counter-clockwise direction. The angle ϕ is measured from the X-direction to the line PQ, and ϕ_0 is the angle before deformation. The variable ψ is used to represent the arc angle, while ζ and θ describe the PRB segment angles and the deformation of each segment, as discussed previously. The sign of ψ is negative if the beam arcs clockwise from P to Q (or is in the interior of the loop) and positive if it is counter-clockwise (or on the exterior of the loop). The following equations are defined for the pth beam

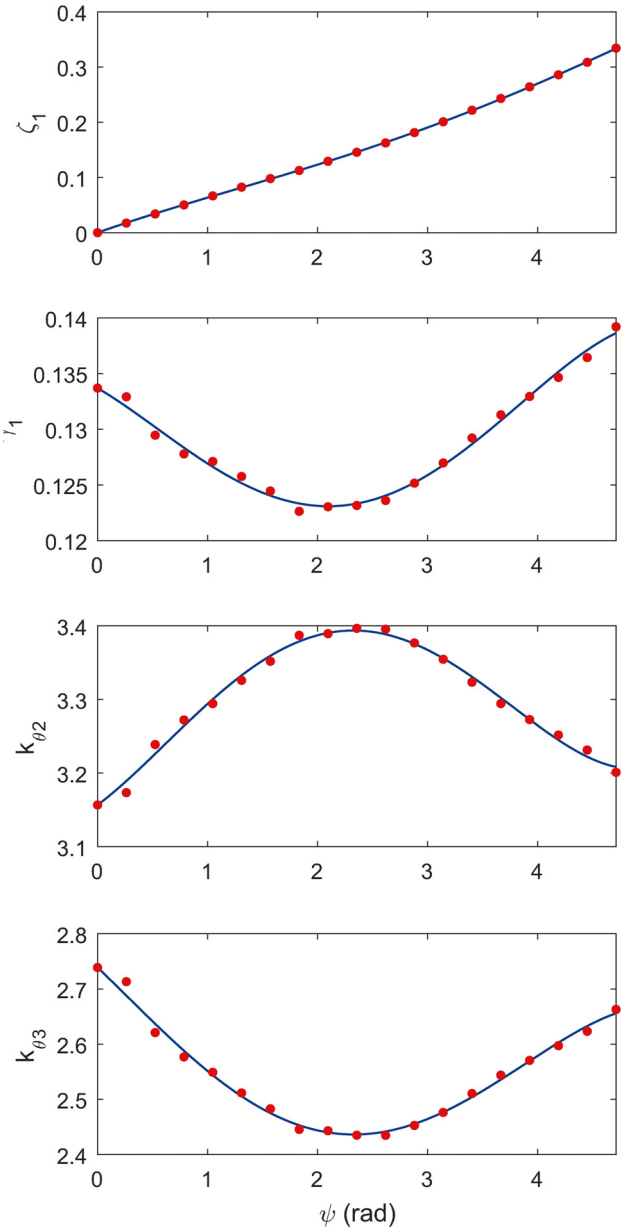

Fig. 4 Plots showing the variation of the optimal PRB parameters as a function of the arc angle, ψ in radians. The result at $\psi = 0$ represents a straight beam. The optimization was performed at 15 deg intervals. The curves are polynomial fitting functions presented at the end of Sec. 2.3.

$$\phi_p = \phi_{0p} + \sum_{j=1}^{p-1}\sum_{k=1}^{n}\theta_{jk} \tag{9}$$

$$\Theta_{pj} = \phi_p - \frac{1}{2}\psi_p + \sum_{k=1}^{j}(\zeta_{pk} + \theta_{pk}) \tag{10}$$

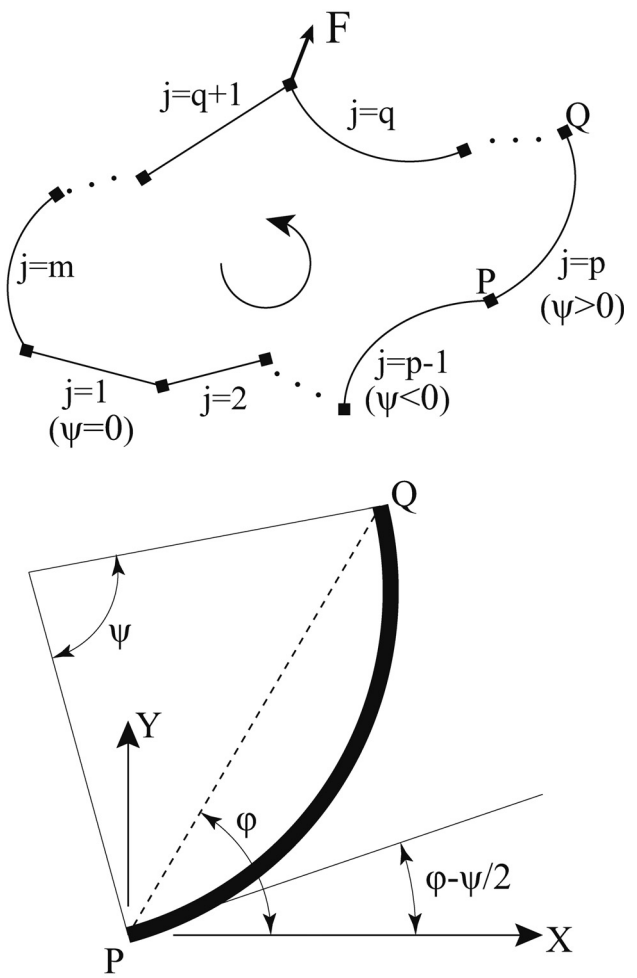

Fig. 5 Schematic of a single-loop compliant mechanism with multiple beams subjected to a load of force F and moment *M* (above) and one beam shown separately for defining variables (below)

where X_{ab} represents any variable X for the ath beam and its bth PRB segment, and n is the number of PRB segments for the beam, so $n = 4$ for all the equations presented here. Θ is the angle of the PRB segment with the horizontal axis. The projections of each beam on the X and Y axes are given by

$$\mathbf{\Gamma}_p = L_p \begin{Bmatrix} \sum_{j=1}^{n}\gamma_{pj}\cos\Theta_j \\ \sum_{j=1}^{n}\gamma_{pj}\sin\Theta_j \end{Bmatrix} \tag{11}$$

where L_p is the length of the pth beam. If the loop has m beams, all rigidly connected to the adjacent members, the kinematic constraints are given by

Table 2 Coefficients of polynomial fits for PRB parameters as a function of the arc angle (ψ) in radians. The expressions are of the form $X(\psi) = C_0 + C_1\psi + C_2\psi^2 + C_3\psi^3 + C_4\psi^4$, where X can be ζ_1, $k_{\theta 2}$ or $k_{\theta 3}$

Parameter	C_0	C_1	C_2	C_3	C_4
ζ_1	0	7.054×10^{-2}	-1.029×10^{-2}	3.440×10^{-3}	-2.642×10^{-4}
$k_{\theta 2}$	3.157	1.117×10^{-1}	5.774×10^{-2}	-3.624×10^{-2}	4.128×10^{-1}
$k_{\theta 3}$	2.739	-1.905×10^{-1}	-2.240×10^{-2}	2.886×10^{-2}	-3.463×10^{-3}

$$\sum_{p=1}^{m} \mathbf{\Gamma}_p = \begin{Bmatrix} 0 \\ 0 \end{Bmatrix} \tag{12}$$

$$\sum_{p=1}^{m} \sum_{k=2}^{n} \theta_{pk} = 0 \tag{13}$$

Let us assume that the mechanism is subjected to a force $\mathbf{F}$ at the end of the qth beam, along with a moment M. This leads to a displacement $\boldsymbol{\delta}$ at that location, and a change in orientation, θ_δ

$$\boldsymbol{\delta} = \sum_{p=1}^{q} \mathbf{\Gamma}_p - \sum_{p=1}^{q} \mathbf{\Gamma}_p \Big|_{\theta_{pk}=0} \qquad k = 1, 2, \ldots n \tag{14}$$

$$\theta_\delta = \sum_{p=1}^{q} \sum_{k=2}^{n} \theta_{pk} \quad k = 1, 2, \ldots n \tag{15}$$

The energy input into the mechanism is given by

$$W_{\text{in}} = \mathbf{F} \cdot \boldsymbol{\delta} + M \cdot \theta_\delta \tag{16}$$

The strain energy in the system, captured by the springs in the PRB models, is the total potential energy of the mechanism

$$V_{\text{total}} = \frac{1}{2} \sum_{p=1}^{m} \sum_{k=2}^{n} K_{\theta k,p}\, \theta_{pk}^2 \tag{17}$$

The residual energy in the mechanism is given by

$$E_{\text{res}} = W_{\text{in}} - V_{\text{total}} \tag{18}$$

The statics solution for the mechanism can be obtained by using a nonlinear optimization routine to minimize the residual energy in the system (Eq. (18)) subject to kinematic constraints (Eqs. (3)–(13)). This has been proven to be a fast and effective method for calculating the deformation of compliant mechanisms using the PRB modeling approach [31].

The equations described above were validated using the example of a compliant mechanism that can be divided into three beam flexures ($m = 3$) as shown in Fig. 6, subjected to a force $\mathbf{F}$ at P_2 ($q = 2$). The parameters of the problem are given in Table 3. The constrained energy minimization calculations were performed in Wolfram Mathematica using an interior-point method, whereby the force F was calculated with the displacement as the input. The results were compared against finite element analysis performed using B21 linear beam elements in ABAQUS. The shape of the PRB model and the results from FEA are overlaid to illustrate how the PRB model is capable of providing insight into the actual deformed state of the flexures. Figure 7 compares the results of the displacement of $\mathbf{P}_2$ over the range of forces described here. The accuracy of the method is demonstrated by the low mean errors in estimating the forces in the X and Y directions of 7.15×10^{-4} N and 6.81×10^{-4} N, respectively.

The methodology described here enables the analysis of fully compliant mechanisms with combinations of initially curved and straight compliant beams. This can also be extended to more complex flexible members, assuming that the PRB models can be incorporated into a similar framework.

4 Case Study: Design of a Constant-Force Mechanism

Constant force mechanisms are a special class of compliant mechanisms that are useful to eliminate the need for complex force control [32]. They are particularly useful in gripping applications to avoid damage to the payload [33]. As the name suggests, they are capable of providing a constant force output over a range of displacement. In this section, the framework

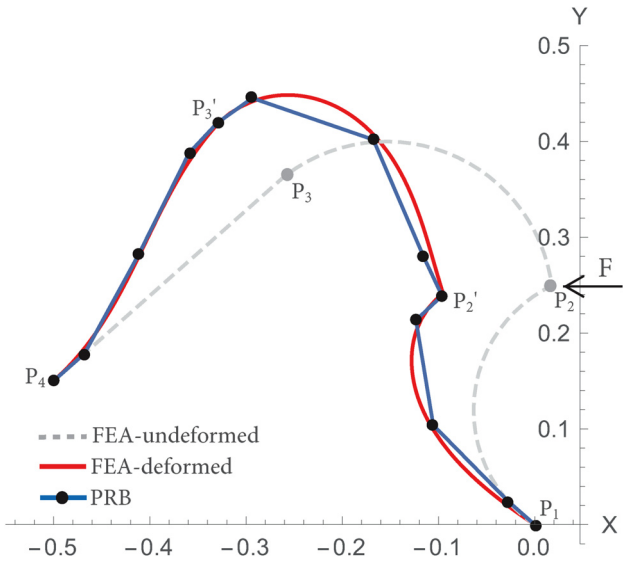

Fig. 6 Shape of a three beam compliant mechanism with two curved and one straight beam calculated using FEA and the PRB model described in this paper

Table 3 Values of the variables for the mechanism shown in Fig. 6. The first three rows are coordinates of the nodes. The third beam has zero curvature (ψ_3=0). The beams are assumed to have unit elastic modulus and unit second moment of area (E=1, I=1).

Variable	Value
P_1	$\{0, 0\}$
P_2	$\{0.018, 0.249\}$
P_3	$\{-0.260, 0.364\}$
P_4	$\{-0.5, 0.15\}$
ψ_1	$-2\pi/3$
ψ_2	$2\pi/3$
ψ_3	0

defined in this paper will be used to develop the initial design for a fully compliant constant force mechanism.

Consider the schematic shown in Fig. 8. It is one half of a symmetric mechanism, which consists of six compliant beams, and the output (force or displacement) is along the line DD', which is also the line of symmetry. There are three beams on either side of the mechanism, which may be straight or curved. Node A is fixed to the ground. For the problem discussed here, the dimensions are

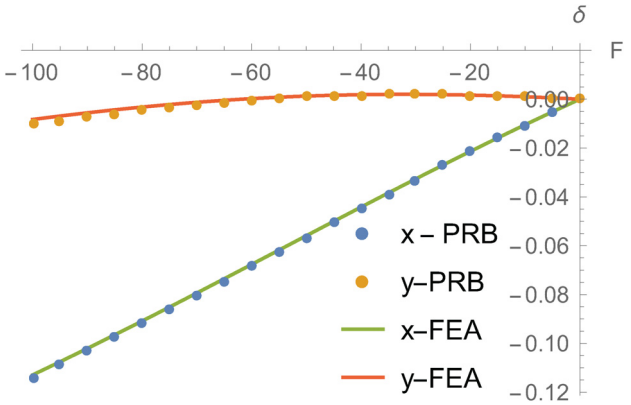

Fig. 7 Comparison of displacement of P_2 from Fig. 6 under the action of load F

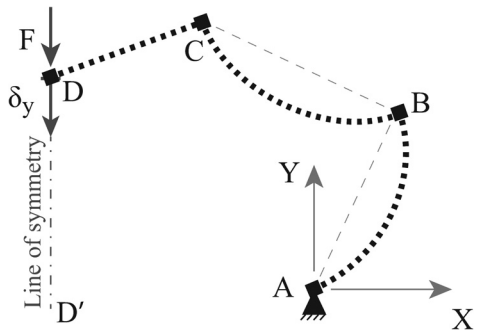

Fig. 8 Schematic of one half of a symmetric compliant mechanism. Each half has three beams, which may be curved or straight. The thick black dotted lines represent one possible topology with two curved beams and one straight beam.

Table 4 Optimal design parameters for constant-force mechanism. The first six rows refer to the coordinates of the nodes. The last two are the ratios of the second moments of area of the second and third beams with respect to the first beam.

Variable	Lower bound	Upper bound	Optimum value
B_x	−0.1	0.1	−0.095
B_y	0.15	0.35	0.312
C_x	−0.35	−.35	−0.246
C_y	0.3	0.5	0.311
D_x	−0.65	−0.45	−0.621
D_y	0.25	0.55	0.491
ψ_1	$-\pi$	π	−0.606
ψ_2	$-\pi$	π	−2.964
ψ_3	$-\pi$	π	−0.856
I_2/I_1	0.5	5	4.704
I_3/I_1	0.5	5	2.355

normalized, and the material has a unit elastic modulus. This allows the designs to be scaled based on the desired application. The beams have uniform cross section along their lengths, defined as I_1, I_2, and I_3, respectively. The variables in the design are the coordinates of the nodes B, C, and D as defined in Fig. 5, the angle of curvature of each beam (ψ_1, ψ_2, and ψ_3), and the ratios of the second moments of area (I_2/I_1 and I_3/I_1).

To check if a given design satisfies the criteria for a constant-force mechanism, the potential energy in the mechanism must be plotted as a function of the displacement, which is the input. Upon differentiating the energy curve, the force required to produce the displacement can be calculated. If the displacement–force curve has a reasonable range over which the force remains constant, the design can be used as a constant-force mechanism.

The analysis is similar to the procedure detailed in Sec. 3. It is assumed that the point D cannot move in the $x-$ direction due to symmetry. The major difference to the example in Sec. 3 is that the objective function for the minimization for the statics solution is just the potential energy in the mechanism, V_{total}, and the displacement along the $y-$ axis, δ_y is the input.

$$\text{Minimize} \quad E(\delta_y) = \frac{1}{2}\sum_{p=1}^{3}\sum_{k=2}^{4} K_{\theta k,p}\,\theta_{pk}^2$$

$$\text{subject to} \quad \sum_{p=1}^{3}\Gamma_p - \sum_{p=1}^{3}\Gamma_p\Big|_{\theta_{pk}=0} = \begin{bmatrix} 0 \\ \delta_y \end{bmatrix}$$

Note that only one half of the mechanism is analyzed due to symmetry. The energy–displacement curve is obtained by varying the displacement δ_y (at discrete points) for the static solution above, and is then differentiated to obtain the force–displacement curve. The standard deviation of the force over the range of displacement is used to determine the variation in the force. For the constant-force mechanism, the design objective is to minimize this variation. The problem definition for the design optimization is given by

$$\underset{\bar{X}}{\text{Minimize}} \quad f(\bar{X}) = \sigma\left(F_y \mid \delta_y \in [\delta_{\min}, \delta_{\max}]\right)$$

$$\text{where} \quad F_y = \frac{dE}{d\delta_y}$$

$$\text{subject to} \quad \bar{X}_{lb} \le \bar{X} \le \bar{X}_{ub}$$

where $\bar{X}$ is the set of design variables, f is the objective function, E and F are the strain energy and associated displacement force, σ represents the standard deviation over the data set, and lb and ub represent lower and upper bounds for the variables, set by the user. $\delta_{\min}$ and $\delta_{\max}$ define the range of motion of the mechanism, which were 0 and −0.4, respectively. The optimization over eleven variables was performed using a genetic algorithm in MATLAB. The bounds of the variables and the results are given in Table 4.

The effectiveness of the PRB model approach in deriving the constant force mechanism was validated using ABAQUS FEA. A screenshot of the final mechanism analyzed with four node, reduced-integration, finite strains shell elements (S4R) is presented in Fig. 9. Note that additional material was added at the points of the intersection of the beams in order to produce a feasible design. The plots of strain energy and force versus displacement obtained from FEA are shown in Fig. 10. The data from the PRB approach are also shown, and the average errors in estimation are 0.36J for the energy and 1.62N for the force. As is

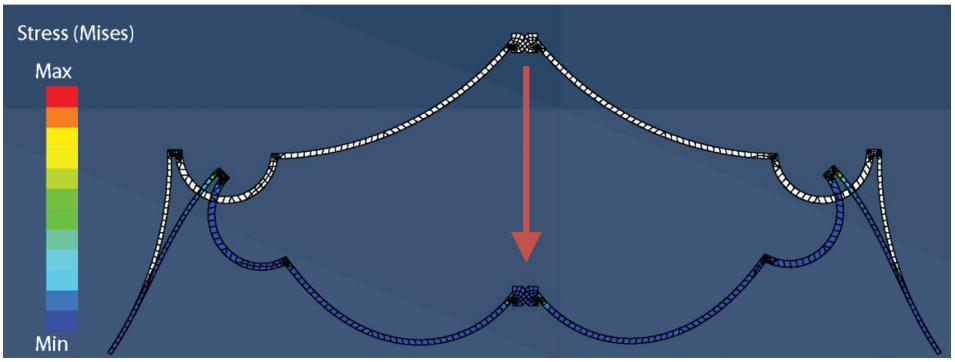

Fig. 9 The optimized version of the constant-force mechanism analyzed using FEA. The undeformed mechanism is shown in white, and the stress variation is illustrated in the deformed mechanism.

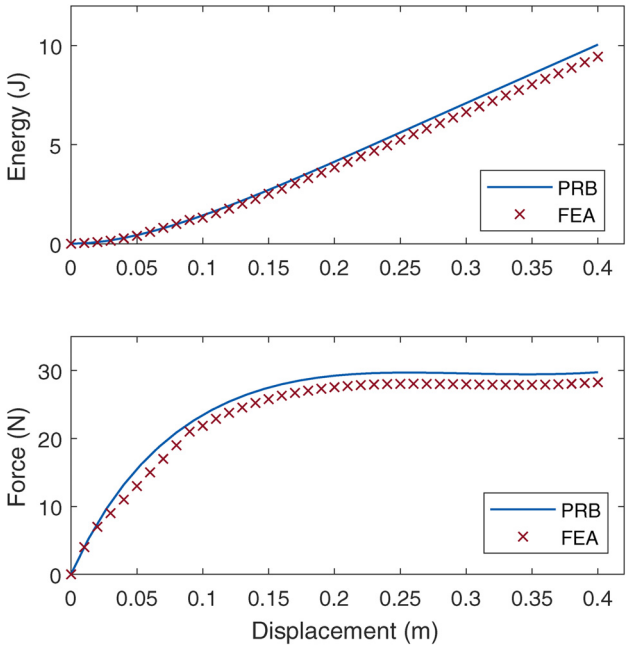

Fig. 10 Comparison of results from FEA and PRB analysis. The plot at the top shows the change in strain energy versus the displacement and the one at the bottom is the plot for force.

noticeable, the FEA results are slightly offset from the PRB data. This can be attributed to the small changes made to the theoretical design obtained from the PRB approach. However, the characteristic constant-force behavior of the mechanism is retained, which demonstrates the efficacy of the methodology described in this paper.

5 Discussion

The PRB model approach allows for easy derivation of equations for the analysis of compliant mechanisms. Through careful optimization of the parameters, it is possible to have highly accurate models that capture the deformation of the beams. The solution process for static equilibrium of the system is also fast with the use of energy approach as illustrated in Sec. 3. It has been demonstrated in literature that PRB models have significant computational advantages over beam equations and finite element methods due to simpler equations, reduced number of unknowns, and the potential for gradient-based numerical solutions [23]. The framework for analysis is presented here in its full form, but can be simplified to a general form using rigid-body transformations.

The 3R PRB model for initially curved beams shown here is versatile because it can encapsulate the bending characteristics of a large range of beam shapes. The loop equations for the compliant beams are also derived with the same idea in mind. Here, the angle of curvature, ψ, is used to define the beams. The models previously defined in literature have been for one specific end being fixed, with loads applied at the other end (see Refs. [17,19], and [20]). This renders those models difficult to use for general design problems, especially for automated design or topology optimization, which is the reasoning behind the symmetry of the model defined in this paper. The approach presented here can be easily extended to include other shapes of flexure elements. For instance, splines can be used for representation of general curves, and the circular segments presented in this work are a specific form of quadratic splines. The methodology can be applied to determine the values of the PRB parameters as functions of the coefficients of the spline polynomials. Other commonly used compliant elements such as small-length flexural pivots can be incorporated into the analysis by using the appropriate values for the PRB parameters in Eqs. (11) and (17).

It is worth noting that in the examples presented in this paper, the beams have been described using exactly circular segments, which may be difficult for other designs. In such cases, the beams must be suitably discretized into arcs for a good approximation. Additionally, only single-loop mechanisms are considered here, and the kinetostatic equations must be altered accordingly for other topologies. The current model is also suited only to systems consisting entirely of thin beam-like elements, where bending characteristics dominate.

The accuracy of the PRB approach in determining both the deflection behavior and the actual shape of the flexure elements is very good, as demonstrated by comparisons to FEA. There is a small error, as noticed in Fig. 10, but it is worth noting that the PRB model approximates the compliant members purely as beam elements. Perhaps more importantly, it gives the designer an easy approach for initial design of the mechanism, which would be beneficial for proving feasibility and checking the proof of concept. In the case of the constant-force mechanism shown here, a workable design is obtained through the method described here. The calculation of stress in the mechanism from PRB models is not detailed in this paper, but it is possible through back-calculation using the bending angles, and has been addressed in Ref. [23].

6 Conclusion

The nature of the definition of PRB models allows them to be extended to model various types of mechanism characteristics. It would be beneficial to the research community to create a uniform formulation to simplify their use. This paper aims to address this issue by bringing a large range of compliant members under the definition of one model with four segments and three revolute joints. The numerical results for the PRB parameters can be adapted to any size range, and the kinematic constraints and statics equations are also easy to implement. With a simple optimization routine and an understanding of beam bending, it was possible to create a framework for analyzing a large variety of compliant mechanisms. The effectiveness of this approach is clearly demonstrated by the fast design of the constant force mechanism.

Funding Data

- National Science Foundation (Grant No. CMMI-1637656).

References

[1] Howell, L. L., 2001, *Compliant Mechanisms*, Wiley, New York.
[2] Howell, L. L., Magleby, S. P., and Olsen, B. M., 2013, *Handbook of Compliant Mechanisms*, Wiley, New York.
[3] Hopkins, J. B., and Culpepper, M. L., 2010, "Synthesis of Multi-Degree of Freedom, Parallel Flexure System Concepts Via Freedom and Constraint Topology (FACT)—Part II: Practice," Precis. Eng., **34**(2), pp. 271–278.
[4] Hopkins, J. B., and Culpepper, M. L., 2010, "Synthesis of Multi-Degree of Freedom, Parallel Flexure System Concepts Via Freedom and Constraint Topology (FACT)—Part I: Principles," Precis. Eng., **34**(2), pp. 259–270.
[5] Kim, C. J., Moon, Y.-M., and Kota, S., 2008, "A Building Block Approach to the Conceptual Synthesis of Compliant Mechanisms Utilizing Compliance and Stiffness Ellipsoids," ASME J. Mech. Des., **130**(2), p. 022308.
[6] Su, H.-J., Dorozhkin, D., and Vance, J., 2009, "A Screw Theory Approach for the Conceptual Design of Flexible Joints for Compliant Mechanisms," ASME J. Mech. Rob., **1**(4), p. 041009.
[7] Su, H.-J., 2011, "Mobility Analysis of Flexure Mechanisms Via Screw Algebra," ASME J. Mech. Rob., **3**(4), p. 041010.
[8] Awtar, S., Slocum, A. H., and Sevincer, E., 2006, "Characteristics of Beam-Based Flexure Modules," ASME J. Mech. Des., **129**(6), pp. 625–639.
[9] Ma, F., and Chen, G., 2015, "Modeling Large Planar Deflections of Flexible Beams in Compliant Mechanisms Using Chained Beam-Constraint-Model," ASME J. Mech. Rob., **8**(2), p. 021018.
[10] Frecker, M. I., Ananthasuresh, G. K., Nishiwaki, S., Kikuchi, N., and Kota, S., 1997, "Topological Synthesis of Compliant Mechanisms Using Multi-Criteria Optimization," ASME J. Mech. Des., **119**(2), pp. 238–245.

[11] Kota, S., Joo, J., Li, Z., Rodgers, S. M., and Sniegowski, J., 2001, "Design of Compliant Mechanisms: Applications to MEMS," Analog Integr. Circuits Signal Process., **29**(1/2), pp. 7–15.
[12] Howell, L. L., and Midha, A., 1994, "A Method for the Design of Compliant Mechanisms With Small-Length Flexural Pivots," ASME J. Mech. Des., **116**(1), pp. 280–290.
[13] Dado, M. H., 2001, "Variable Parametric Pseudo-Rigid-Body Model for Large-Deflection Beams With End Loads," Int. J. Non-Linear Mech., **36**(7), pp. 1123–1133.
[14] Saxena, A., and Kramer, S. N., 1998, "A Simple and Accurate Method for Determining Large Deflections in Compliant Mechanisms Subjected to End Forces and Moments," ASME J. Mech. Des., **120**(3), pp. 392–400.
[15] Kimball, C., and Tsai, L.-W., 2002, "Modeling of Flexural Beams Subjected to Arbitrary End Loads," ASME J. Mech. Des., **124**(2), pp. 223–235.
[16] Edwards, B. T., Jensen, B. D., and Howell, L. L., 1999, "A Pseudo-Rigid-Body Model for Initially-Curved Pinned-Pinned Segments Used in Compliant Mechanisms," ASME J. Mech. Des., **123**(3), pp. 464–468.
[17] Venkiteswaran, V. K., and Su, H.-J., 2016, "Pseudo-Rigid-Body Models for Circular Beams Under Combined Tip Loads," Mech. Mach. Theory, **106**, pp. 80–93.
[18] Pei, X., Yu, J., Zong, G., and Bi, S., 2010, "An Effective Pseudo-Rigid-Body Method for Beam-Based Compliant Mechanisms," Precis. Eng., **34**(3), pp. 634–639.
[19] Su, H.-J., 2009, "A Pseudorigid-Body 3r Model for Determining Large Deflection of Cantilever Beams Subject to Tip Loads," ASME J. Mech. Rob., **1**(2), p. 021008.
[20] Yu, Y.-Q., Feng, Z.-L., and Xu, Q.-P., 2012, "A Pseudo-Rigid-Body 2r Model of Flexural Beam in Compliant Mechanisms," Mech. Mach. Theory, **55**, pp. 18–33.
[21] Venkiteswaran, V. K., and Su, H.-J., 2016, "A Three-Spring Pseudorigid-Body Model for Soft Joints With Significant Elongation Effects," ASME J. Mech. Rob., **8**(6), p. 061001.
[22] Venkiteswaran, V. K., and Su, H.-J., 2016, "Extension Effects in Compliant Joints and Pseudo-Rigid-Body Models," ASME J. Mech. Des., **138**(9), p. 092302.
[23] Venkiteswaran, V. K., Turkkan, O. A., and Su, H.-J., 2017, "Speeding Up Topology Optimization of Compliant Mechanisms With Pseudo-Rigid-Body Models," ASME J. Mech. Rob., **9**(4), p. 041007.
[24] Lu, K.-J., and Kota, S., 2005, "An Effective Method of Synthesizing Compliant Adaptive Structures Using Load Path Representation," J. Intell. Mater. Syst. Struct., **16**(4), pp. 307–317.
[25] Roach, G. M., and Howell, L. L., 2002, "Evaluation and Comparison of Alternative Compliant Overrunning Clutch Designs," ASME J. Mech. Des., **124**(3), pp. 485–491.
[26] Qiu, J., Lang, J., and Slocum, A., 2004, "A Curved-Beam Bistable Mechanism," J. Microelectromech. Syst., **13**(2), pp. 137–146.
[27] Wang, N., Liang, X., and Zhang, X., 2014, "Pseudo-Rigid-Body Model for Corrugated Cantilever Beam Used in Compliant Mechanisms," Chin. J. Mech. Eng., **27**(1), pp. 122–129.
[28] Midha, A., Kuber, R. S., and Bapat, S. G., 2015, "Development of a Methodology for Pseudo-Rigid-Body Models of Compliant Beams With Inserts, and Experimental Validation," ASME. International Design Engineering Technical Conferences and Computers and Information in Engineering Conference (Volume 5A: 39th Mechanisms and Robotics Conference), Boston, MA, Aug 2–5.
[29] Venkiteswaran, V. K., and Su, H.-J., 2015, "A Parameter Optimization Framework for Determining the Pseudo-Rigid-Body Model of Cantilever-Beams," Precis. Eng., **40**, pp. 46–54.
[30] Craig, J. J., 2005, *Introduction to Robotics: Mechanics and Control*, Pearson Education, Incorporated, London.
[31] Turkkan, O. A., and Su, H.-J., 2016, "DAS-2d: A Concept Design Tool for Compliant Mechanisms," Mech. Sci., **7**(2), pp. 135–148.
[32] Boyle, C., Howell, L. L., Magleby, S. P., and Evans, M. S., 2003, "Dynamic Modeling of Compliant Constant-Force Compression Mechanisms," Mech. Mach. Theory, **38**(12), pp. 1469–1487.
[33] Chen, Y.-H., and Lan, C.-C., 2012, "An Adjustable Constant-Force Mechanism for Adaptive End-Effector Operations," ASME J. Mech. Des., **134**(3), p. 031005.